JOURNAL OF MATERIALS SCIENCE 18 (1983) 804–814

Crystallization of amorphous $Ni_{60}Nb_{40}$

L. E. COLLINS*, N. J. GRANT, J. B. VANDER SANDE
Department of Materials Science and Engineering, Massachusetts Institute of Technology, Cambridge, MA 02139, USA

The crystallization of $Ni_{60}Nb_{40}$ metallic glass during continuous heating and isothermal annealing at temperatures from 845 to 904 K, was studied by differential scanning calorimetry (DSC), electrical resistance measurements, X-ray diffraction and transmission electron microscopy. Crystallization occurred in four clearly defined stages. In the initial stage a metastable phase, with structure similar to the M-phase in the Ni–Nb–Al ternary system, forms in the amorphous matrix. In the two subsequent stages the remaining glass crystallizes to the Ni_3Nb- and μ-phases found in the equilibrium Ni–Nb phase diagram. The M-phase transforms into the equilibrium Ni_3Nb- and μ-phases only at high temperature. The crystallization of the M-phase could be described by Johnson–Mehl–Avrami kinetics with the time exponent $n = 1.3$ and activation energy $E_1 = 628\,kJ\,mol^{-1}$. M-phase crystal growth was apparently diffusion controlled and the diffusion coefficient was estimated to be $4.2 \times 10^{-20}\,m^2\,sec^{-1}$. Activation energies for the second and third stages of crystallization were found to be $E_2 = 446\,kJ\,mol^{-1}$ and $E_3 = 430\,kJ\,mol^{-1}$.

1. Introduction

The crystallization of metallic glasses is a topic of considerable interest. Technologically, the subject is of importance since the properties of the glass may be changed significantly by the onset of crystallization, and the utilization of the glass is thus limited by the conditions of time and temperature at which crystallization occurs. Scientifically, the crystallization of metallic glasses provides an opportunity to study the nucleation and growth of crystalline phases under conditions far removed from equilibrium.

To date, although there have been numerous studies of crystallization behaviour of metal–metalloid glasses, few studies of metal–metal glasses have been reported. The purpose of the present study was to examine in detail the crystallization of the amorphous $Ni_{60}Nb_{40}$ alloy. This behaviour has been treated briefly in previous papers [1, 2] and the intent of the present work is to examine in greater detail the structural changes occurring during crystallization using X-ray diffraction and transmission electron microscopy (TEM). Transformation kinetics were determined over a wide temperature range using electrical resistance measurements and differential scanning calorimetry (DSC).

2. Experimental details

Amorphous ribbons were prepared by a melt spinning technique. 10 g buttons of the alloy $Ni_{60}Nb_{40}$ were prepared by melting appropriate quantities of nickel and niobium (99.95% and 99.9% purity, respectively) in a nonconsummable vacuum arc furnace. After repeated melting to ensure chemical homogeneity the buttons were placed in an alumina crucible through the base of which a 1 mm pouring hole had been drilled. The charge was heated by induction in a helium atmosphere to 1675 K and the molten metal was ejected using a pressure of 55 kPa onto the inner rim surface of a copper wheel rotating at 40 m sec^{-1}. The ribbons produced in this manner averaged 30 to 40 μm in thickness and 2 mm in width. X-ray and TEM examinations failed to reveal any evidence of crystallinity in the as-quenched ribbons.

Differential scanning calorimetry experiments were carried out on a Perkin-Elmer DSC-2 calorimeter. The temperature scale was calibrated to

*Present address: Metallurgy Section, Canada Centre for Minerals and Energy Technology, Ottawa, Ontario, Canada.

0022–2461/83/030804–11$03.82/0 © *1983 Chapman and Hall Ltd.*

within ± 1 K using K_2SO_4 and K_2CrO_4 standards and baseline sensitivity of 5 mcal sec^{-1}. The samples (typically 4 to 6 mg) were contained in graphite pans; alumina was used as a reference material. Heating rates from 1 to 80 K min^{-1} were used.

Annealing kinetics were determined from isothermal electrical resistance measurements using a four-point probe system in which platinum leads were spot welded to the 2 cm long samples. The assembly was enclosed in a Vycor tube which was then evacuated prior to heating in a resistance tube furnace. Once placed in the furnace, the sample came to temperature in approximately 10 min; throughout the remainder of the experiment the temperature varied by less than ± 1.5 K. A constant current of approximately 5 mA was maintained throughout the experiment. A strip chart recorder was used to monitor electrical resistance as a function of time during each of the 13 tests performed at temperatures between 845 and 905 K.

In order to determine the structural changes indicated by the observed variations in resistance, samples were encapsulated in evacuated Vycor tubes and isothermally annealed for various times at 871 K. Subsequent to annealing the samples were examined by X-ray diffraction and TEM. The thin foils for TEM observations were prepared by a window technique in which the samples were electropolished at 54 V in a bath of 10% H_2SO_4 in methanol at 223 K. The thinned samples were examined in a Philips EM 300 microscope. A number of the isothermally annealed samples were scanned in the DSC to determine if the structural relaxation expected during annealing would alter the crystallization process in any way.

3. Results

3.1. DSC measurements

A typical DSC scan of the as-quenched $Ni_{60}Nb_{40}$ is shown in Fig. 1. At a heating rate $\beta = 20$ K min^{-1} three distinct exothermic peaks are observed at 940, 980 and 994 K. The initial crystallization exotherm obscures the glass transition, but at higher heating rates a decrease in heat capacity, typical of the glass transition, was evident prior to the onset of crystallization. The calorimeter was limited to a maximum temperature of 1000 K and consequently the third peak is incomplete. It is not clear from the DSC results if further

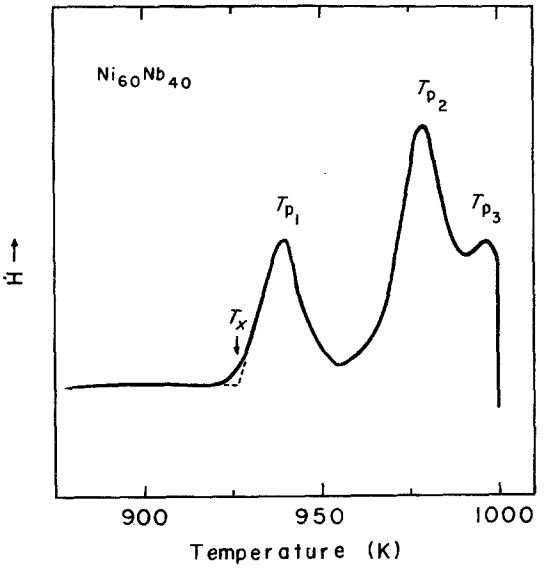

Figure 1 DSC thermogram obtained at heating rate $\beta = 20$ K min^{-1}.

transformations would occur at higher temperature.

Using the method of Kissinger [3], the apparent activation energy for each step of the crystallization process was obtained from the slope of a plot of log (T_p^2/β) against $1/T$ (Fig. 2), where T_p is the peak temperature in the DSC thermogram obtained at heating rate β. The deviation from linearity at high heating rates is probably due to

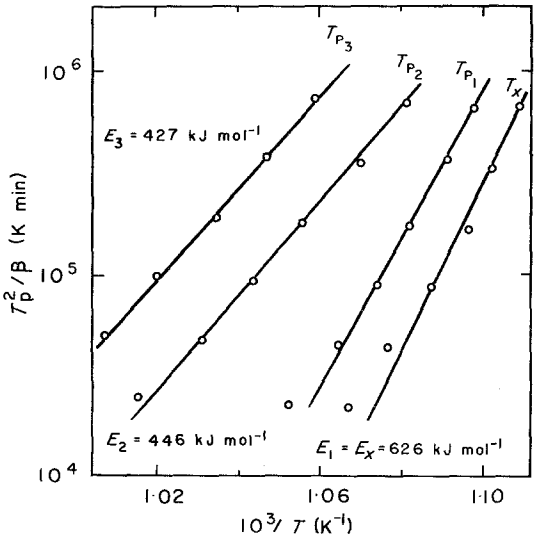

Figure 2 Plot of T_p^2/β against $1/T$ for the three crystallization peaks observed in the DSC scans of $Ni_{60}Nb_{40}$ samples. Also shown is the temperature of the onset of crystallization (T_X).

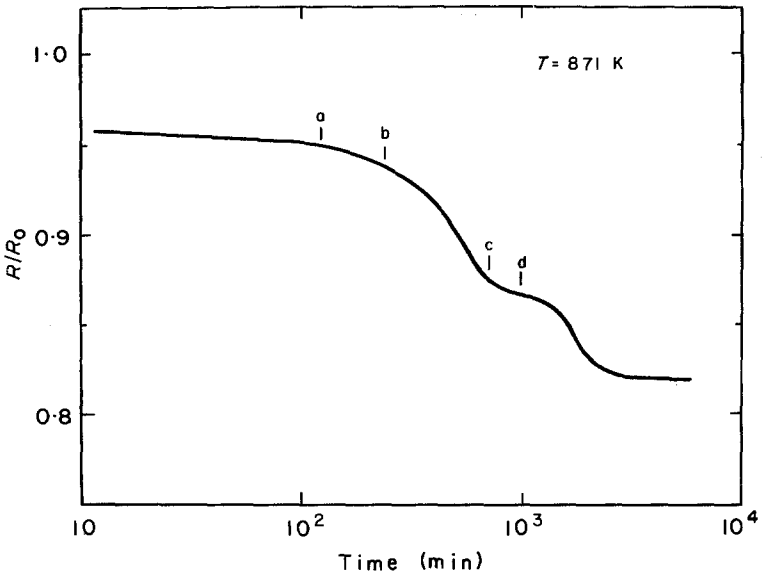

Figure 3 The time dependence of the normalized resistance (R/R_0) during isothermal annealing of $Ni_{60}Nb_{40}$ at 871 K. Letters a to d mark the times of the TEM micrographs shown in Fig. 4.

temperature lags and peak shape distortions in the recording system, as has been discussed by Leake and Greer [4]. For this reason the line through the data points is drawn to show the best fit with those points obtained at lower heating rates. Activation energies for the three stages of crystallization were $E_1 = 626$, $E_2 = 446$ and $E_3 = 427\,\text{kJ mol}^{-1}$. Also included in Fig. 2 is the heating rate dependence of the temperature at the onset of crystallization (T_X), which is seen to follow parallel to the results for the first crystallization peak, suggesting that the same mechanism is responsible for the rate limiting step in both the incubation and the growth periods.

3.2. Resistance measurements

Measurement of electrical resistance provided a very sensitive means of following structural changes. In order to compare the results of tests at different temperatures the resistance R was normalized against the resistance measured at room temperature prior to annealing (R_0) and results are presented as normalized resistance R/R_0. The isothermal resistance measurements at 871 K, shown in Fig. 3, are typical of the results obtained at all temperatures. The features of the curve are similar to those observed by Güntherodt *et al.* [5] in a constant heating rate experiment. Initially there is a very gradual drop in resistance which appeared to be linear with log time. Samples annealed less than 120 min revealed no evidence of crystallinity when examined by X-ray or TEM, suggesting that the initial drop was due to structural relaxation of the glass. After 120 min at 871 K the resistance began to drop more rapidly, indicating the onset of the first stage of crystallization. X-ray diffraction of a sample annealed 720 min at 871 K (point C in Fig. 3) revealed sharp diffraction lines superimposed on the broad diffraction peak of the amorphous material. The interatomic spacings of the crystalline phase are compared in Table I with those of the equilibrium M-phase [6] observed in the ternary Ni–Nb–Al system [7] and are found to be in good agreement.

The second crystallization event appeared to be associated with the intermediate plateau in the resistance measurements. X-ray examination of samples annealed in this region indicated the

TABLE I Crystalline interplanar spacings of the metastable phase observed during stage 1 crystallization of $Ni_{60}Nb_{40}$ glass and of the equilibrium M-phase found in the Ni–Nb–Al ternary system

Observed d (nm)	M-phase (nm)
0.2588	0.2611
	0.2469
0.2386	0.2362
0.2290	0.2307
0.2237	0.2241
0.2201	0.2212
0.2158	0.2169
	0.2111
	0.2058
	0.2049
0.1981	0.1989
	0.1924

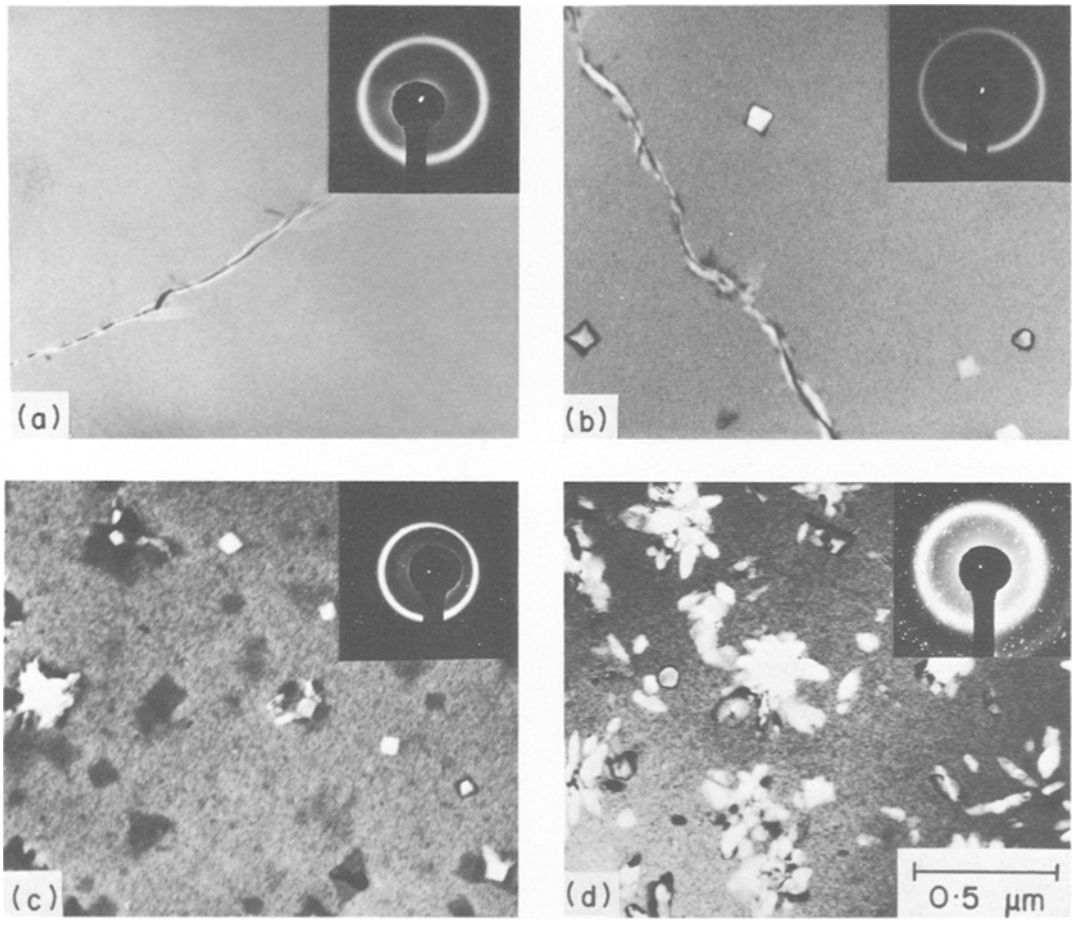

Figure 4 TEM micrographs showing the initial stages of crystallization in $Ni_{60}Nb_{40}$ at 871 K. Values of X calculated from resistance measurements are indicated. (a) 120 min, $X = 0.01$, (b) 240 min, $X = 0.11$, (c) 720 min, $X = 0.60$, and (d) 1000 min.

presence of the Ni_3Nb-phase found in the equilibrium Ni–Nb phase diagram, forming at the expense of the amorphous material, while the M-phase remained unchanged. At the end of the plateau the structure consisted of the amorphous, Ni_3Nb-, and M-phases.

The third crystallization event, indicated by the second decrease in resistance, involved the transformation of the remaining glass into the equilibrium μ(NiNb) phase found in the Ni–Nb phase diagram at 50 to 54 at% Nb. X-ray diffraction confirmed that the material was completely crystalline after 2800 min at 871 K and that the structure consisted of the M-, Ni_3Nb- and μ-phases. The M-phase proved to be very stable and was only transformed to the equilibrium phases after annealing at much higher temperatures (1050 to 1100 K).

The series of TEM micrographs (Fig. 4) shows the initial stages of crystallization in greater detail. After 120 min at 871 K (Fig. 4a) the material appears featureless and the diffraction pattern exhibits only the broad diffuse rings typical of an amorphous material. It will be noted that the ribbon was embrittled by annealing and cracks were often observed in the foils thinned from annealed material. The embrittlement phenomena will be examined more closely in a subsequent paper. At 240 min several widely scattered crystals are evident, ranging in size from 30 to 130 nm. At 720 min the number of crystals has continued to increase and the largest crystals are between 200 and 250 nm in size. Some of the larger crystals developed a rosette shape similar to that observed during the initial stages of dendritic growth [8].

At 720 min there is evidence of the heterogeneous nucleation of the Ni_3Nb-phase at the

glass-crystal interface of some of the larger M-phase crystals. After 1000 min large cellular grains of the Ni_3Nb extend from a large number of the original M-phase crystals.

3.3. Crystallization kinetics

The isothermal crystallization kinetics were analysed in terms of the generalized theory of phase transformations [9] in which the fraction transformed $X(t)$ at time t is given by

$$X(t) = 1 - \exp(-bt^n) \quad (1)$$

where n is an exponent dependent upon the nucleation and growth mechanisms and b is a rate constant assumed to obey a simple Arrhenius law

$$b = b_0 \exp(-\Delta H/kT) \quad (2)$$

where ΔH is the activation energy, k is the Boltzmann constant and T is the absolute temperature.

In the present study it was assumed that $X(t)$ was directly proportional to the change in resistance and thus

$$X(t) = \frac{R_0 - R}{R_0 - R_f} \quad (3)$$

where R_0 is taken as the point at which the resistance first deviates from the log time kinetics of the initial relaxation period and R_f is the resistance after completion of stage 3 of the transformation. Time $t = 0$ is taken to be the end of the incubation period.

Activation energies for stages 1 and 3 were deduced from the temperature dependence of the time to 25% ($t_{X=0.25}$) and 85% ($t_{X=0.85}$) crystallization, respectively, (Fig. 5), by rearrangement of Equations 1 and 2 to give

$$\ln(t_X) = A + (E/kT) \quad (4)$$

where A is a constant and E is an effective activation energy $E = \Delta H/n$. The times $t_{X=0.25}$ and $t_{X=0.85}$ correspond approximately to the midpoints in the resistance drops associated with the transformations. The activation energies, as determined from the slopes of the plots in Fig. 5 ($E_1 = 629\,kJ\,mol^{-1}$ and $E_3 = 433\,kJ\,mol^{-1}$), are compared to those obtained by DSC measurements in Table II and are seen to be in good agreement. Due to the small changes in resistance during the second stage of crystallization it was not possible to make a reliable estimate of E_2 from resistance measurements.

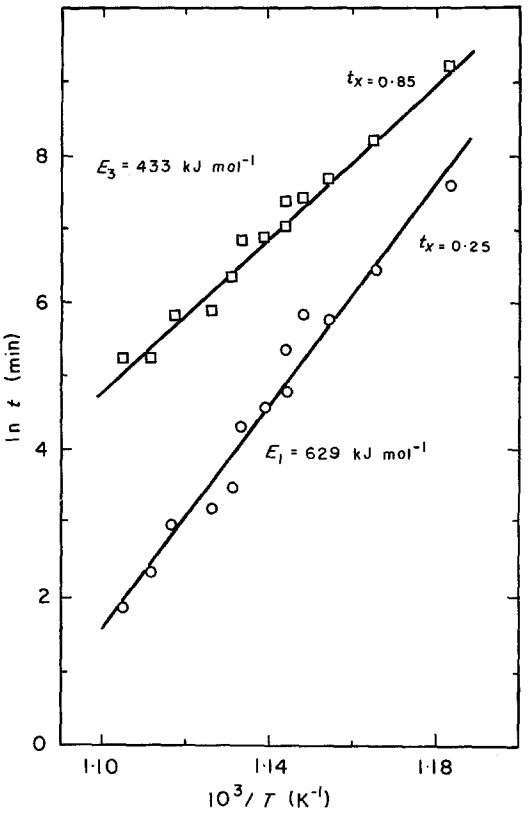

Figure 5 Plots of $\ln t_{X=0.25}$ and $\ln t_{X=0.85}$ against reciprocal temperature determined during isothermal annealing of $Ni_{60}Nb_{40}$.

The time exponent for the first stage of crysallization n may be determined by rewriting Equation 1 in the form of the Johnson–Mehl–Avrami equation:

$$\ln[-\ln(1-X)] = \ln(b) + n\ln(t) \quad (5)$$

Plots of $\ln[-\ln(1-X)]$ against $\ln(t)$, as shown in Fig. 6, are linear for $X \lesssim 0.4$. At $X > 0.4$ deviation from linearity occurs due to the onset of the second stage of crystallization. The values of the time exponent, given by the slopes of the plots, are listed in Table III. The values are independent of temperature and average $n = 1.3 \pm 0.1$.

The application of resistance measurements

TABLE II Comparison of activation energies determined by DSC and resistance measurements

Method	Activation energy (kJ mol^{-1})		
	E_1	E_2	E_3
DSC	626	446	427
Resistance	629	–	433

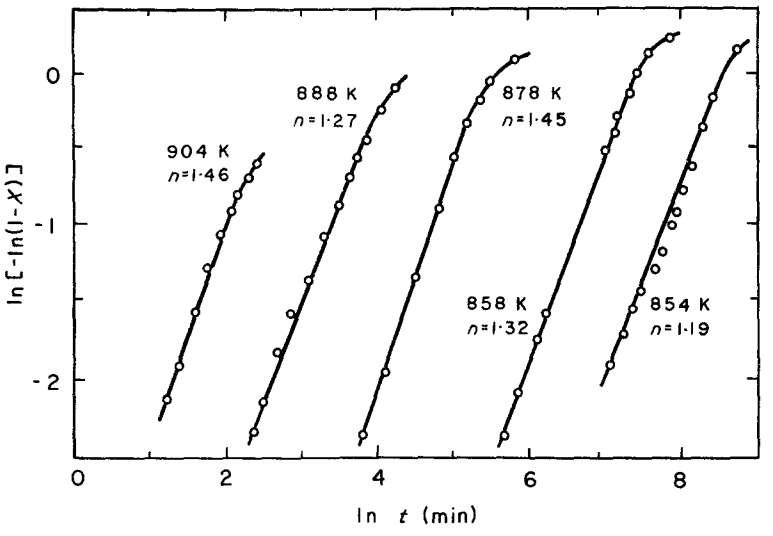

Figure 6 Plot of ln $[-\ln (1-X)]$ against ln t for the initial stage of crystallization of $Ni_{60}Nb_{40}$.

to the determination of crystallization kinetics hinges on the assumption that the fractional change in resistance is directly related to the fraction of the glass which has crystallized. Such an assumption is particularly questionable in a glass such as $Ni_{60}Nb_{40}$ where more than one phase is formed during crystallization since each phase is likely to effect the resistance differently. Such a consideration is unimportant in the determination of activation energies where it is not necessary to know the fraction transformed provided it may be assumed that, for a given fractional change in the resistance, the fraction transformed is fixed. This same assumption is made in determining activation energies from DSC experiments using the Kissinger analysis [10] and the good agreement between the results obtained by the two methods supports the validity of the technique.

TABLE III Time exponent (n) measured during the initial stage of crystallization of $Ni_{60}Nb_{40}$

Temperature (K)	n
845	1.19
858	1.23
871	1.50
874	1.21
874	1.29
878	1.45
882	1.29
884	1.02
895	1.30
899.5	1.27
904	1.46

Average $n = 1.30$

In order to determine the value of the time exponent n it was necessary to be able to calculate X at any time t; the assumptions used are somewhat questionable in view of the obvious phase dependence of resistance. It is noted, however, that the values calculated for X appear to give reasonable estimates of the fraction transformed during stage 1 as seen in Fig. 4. It is also noted that the slope of the ln $[-\ln (1-X)]$ against ln (t) plot is quite insensitive to the actual value of X provided that X is proportional to the fractional change in resistance; thus an error of 50% in the values of X results in a difference of only 0.1 in the value determined for n. As will be seen in the subsequent discussion, such a difference will not significantly alter the interpretation of the process mechanism.

3.4. Crystal growth

Growth rates for the M-phase may be determined from the series of TEM micrographs in Fig. 4. The time dependence of M crystal size is shown in Fig. 7. The size (S) is the largest dimension of the largest crystal observed at time t. It is assumed that smaller crystals nucleated later in the transformation. For diffusion-controlled growth of a spherical particle Aaron *et al.* [11] have shown that the radius S is related to the time t by the expression

$$S = \alpha (Dt)^{1/2} \qquad (6)$$

where D is the apparent diffusion coefficient and α is a dimensionless parameter determined by the composition at the particle interface, the composition of the crystallizing phase, and the initial

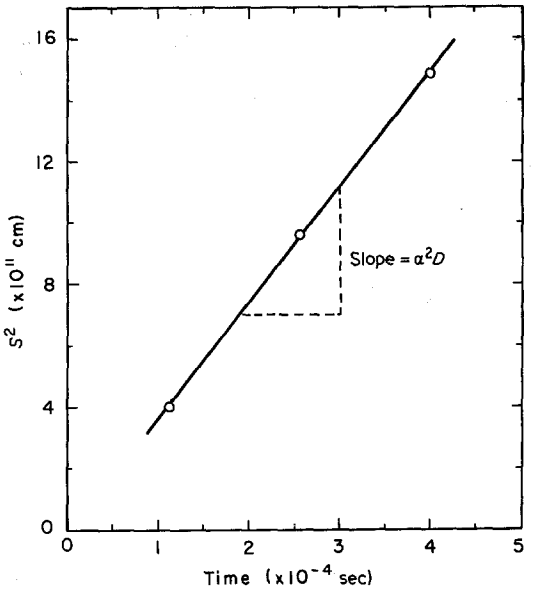

Figure 7 Plot of S^2 against time for the initial stage of crystallization of $Ni_{60}Nb_{40}$, where S is the crystal size.

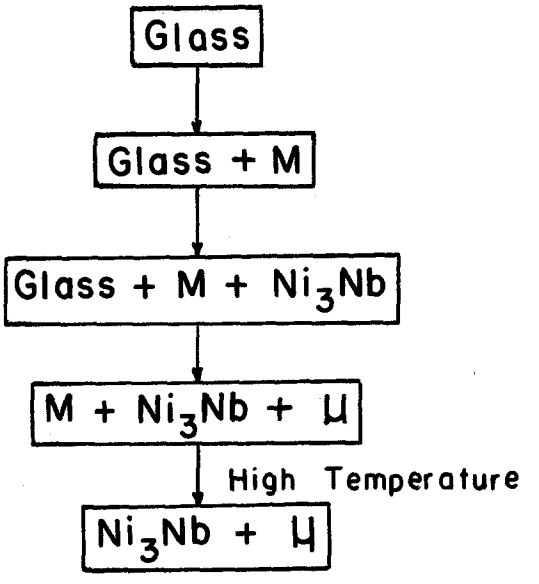

Figure 8 Crystallization sequence of $Ni_{60}Nb_{40}$. The μ- and Ni_3Nb-phases are equilibrium intermetallic phases in the Ni–Nb binary system. The M-phase is metastable and decomposes at high temperature.

composition of the glass. It is apparent from Fig. 7 that this relation is applicable to the present study.

From the slope of the plot of S^2 against t it is possible to obtain an order of magnitude estimate of the diffusion coefficient. If it is assumed that the interface composition is 25 at% Nb (this composition is indicated by the subsequent nucleation of Ni_3Nb) and that the crystal composition is 48 at% Nb (in agreement with the composition of the M-phase), α is estimated in the manner of Aaron *et al.* to equal 3.0. The diffusion coefficient is then found to be $D = 4.2 \times 10^{-20}$ m^2 sec^{-1}. Although the equations used are strictly applicable for growth of a spherical particle, the error, introduced through the value assigned to α, is likely sufficiently small that the value obtained is a reasonable estimate of the order of magnitude.

3.5. Isothermal annealing

No significant changes were noted in the DSC thermograms of samples previously annealed at 871 K for $t < t_X$. The peak positions remained constant for all heat treatments. For annealing times $t > t_X$ the magnitude of the first peak gradually decreased as crystallization proceeded. The first peak was almost completely eliminated at $t = 1000$ min which corresponds to the time at which the resistance measurements indicate that the first stage of crystallization is complete, thus providing further verification that the resistance and DSC measurements are sensitive to the same structural changes.

4. Discussion

4.1. Crystallization

The sequence of crystallization events in $Ni_{60}Nb_{40}$ is summarized in Fig. 8. In the past there was some question as to the structure of the first phase to crystallize. Although formation of a tetragonal phase with lattice parameters $a = 0.1106$ nm and $c = 0.2664$ nm similar to the Ni_2Ta phase found in the equilibrium Ni–Ta system has been reported [12], the present results support the initial findings of Ruhl *et al.* [1] in which the structure of the metastable phase was identified as being similar to that of the equilibrium M-phase in the Ni–Nb–Al system. In that system the σ-like M is found over a range of low aluminium ($\lesssim 20$ at%) compositions containing a constant niobium content of approximately 48 at% [7]. Under the nonequilibrium conditions present during the crystallization of the $Ni_{60}Nb_{40}$ glass a metastable extension of the ternary M-phase region to the binary Ni–Nb system is observed.

In order to understand better the crystallization reactions in the Ni–Nb system it is useful

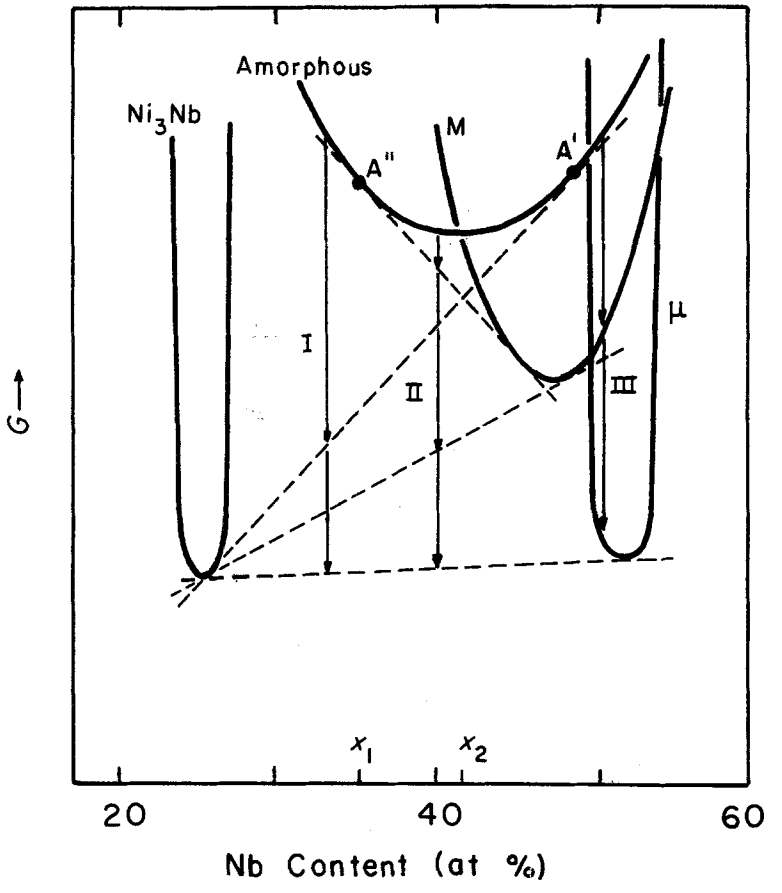

Figure 9 Hypothetical free energy against composition curves illustrating crystallization processes in the Ni–Nb system. Sequence I: $A \rightarrow Ni_3Nb + A' \rightarrow Ni_3Nb + \mu$. Sequence II: $A \rightarrow M + A'' \rightarrow M + Ni_3Nb + A \rightarrow M + Ni_3Nb + \mu \rightarrow Ni_3Nb + \mu$ Sequence III: $A \rightarrow M \rightarrow \mu$.

to consider a schematic diagram of the free energy of the various phases against concentration as shown in Fig. 9. Included in the diagram are free energy plots for the equilibrium Ni_3Nb- and μ-phases, the metastable M, and the amorphous alloy. Based on the position of the M-phase field in the Ni–Nb–Al system, the free energy plot for M might be expected to exhibit a broad minimum centered at approximately 48 at% Nb. The dotted tangents indicate possible metastable equilibria.

It is evident from Fig. 9 (Sequence II) that the free energy of $Ni_{60}Nb_{40}$ glass may be reduced by the formation of M and a Ni-rich glass (A''). Although the free energy change in the formation of M may be small compared to that for the formation of the equilibrium phases ($\Delta G_M < \Delta G_{Ni_3Nb}$, ΔG_μ) consideration of the critical free energy ΔG^* for homogeneous nucleation [13]

$$\Delta G^* = \frac{16\,\pi\,\sigma^2}{3\,\Delta G^3} \qquad (7)$$

suggests this phase may be kinetically favoured because it presents an interface of lower surface energy $\sigma_{M,A}$ than either of the equilibrium phases, i.e. $\sigma_{M,A} < \sigma_{Ni_3Nb,A}$, $\sigma_{\mu,A}$. In the DSC thermograms there is little overlap of the first and second peaks indicating that the reaction $A \rightarrow A'' + M$ goes to completion prior to the onset of stage 2. Transformation of the remaining glass A'' to a metastable equilibrium between the Ni_3Nb and M-phases further reduces the free energy. It is apparent from the overlapping of the second and third peaks of the DSC thermograms that this transformation does not go to completion prior to the onset of stage 3. Although further nucleation of M is expected to accompany formation of Ni_3Nb, transformation to the μ-phase is observed. At this point μ may nucleate heterogeneously at Ni_3Nb/glass interfaces and is thus able to form preferentially to the less stable M. The transformation of M to the equilibrium phases at high temperature has not been studied in detail and it is not clear whether M simply undergoes a polymorphous transformation to the μ-phase of the same composition, or whether the transformation of M is a more complex process involving the formation of both the μ- and Ni_3Nb-phases.

TABLE IV Comparison of activation energies and crystallization temperatures (T_X) of various glasses

Glass	Activation energy (kJ mol^{-1})	T_X (K)	Reference
$Ni_{60}Nb_{40}$	629	927	–
$Ni_{75}P_{16}B_6Al_3$	649	700	[18]
$Cu_{60}Zr_{40}$	560	785	[16]
$Fe_{40}Ni_{40}P_{14}B_6$	367	694	[17, 19]
$Pd_{80}Si_{20}$	334	690	[20]
$Fe_{32}Ni_{36}Cr_{14}P_{12}B_6$	286	656	[19]
$Fe_{80}B_{20}$	241	693	[4]
$Ti_{50}Be_{40}Zr_{10}$	269	683	[21]

In glassy alloys of high niobium content, $X > X_2$, a polymorphous transformation of the glass to the metastable M (Sequence III) would be expected; in fact it has been observed [14, 15] that amorphous $Ni_{50}Nb_{50}$ transforms completely to M prior to transformation to the equilibrium μ. In alloys of low niobium content, $X < X_1$, there is no free energy advantage in the formation of M and alloys will transform to the equilibrium phases (Sequence I) without initial formation of M. In confirmation, recent work [15] has shown that $Ni_{65}Nb_{35}$ glass crystallizes to the equilibrium phases by a two-stage process in which a large fraction of the glass transforms to Ni_3Nb prior to the transformation of the remaining Ni-depleted glass (A′) to μ.

4.2. Crystallization kinetics

The effective activation energy for the first stage of crystallization ($E_1 = 628\,kJ\,mol^{-1}$) determined by both DSC and resistivity experiments is somewhat larger than the value of $600\,kJ\,mol^{-1}$ determined by Pratten and Scott [16] in constant heating rate DSC experiments. These results are judged to be in good agreement in view of the fact that the present results have shown that the measured value of E_1 in DSC experiments is somewhat dependent upon the heating rate, probably due to temperature lag in the recording system. The use of isothermal resistivity measurements to determine activation energy eliminates the effects of temperature lag found in DSC results, and thus should give the better estimate of activation energy.

It is evident from Table IV that the effective activation energy ($E_1 = 628\,kJ\,mol^{-1}$) for the crystallization of the M phase in $Ni_{60}Nb_{40}$ is among the highest of any of the metallic glasses studied to date and is an indication of the high thermal stability of this alloy. The effective activation energy of crystallization is determined by both nucleation and growth processes, each of which is likely to exhibit a different temperature dependence. Since both nucleation and growth clearly occur simultaneously during the formation of M crystals in the $Ni_{60}Nb_{40}$ glass it is not possible to attach physical significance to the value of the activation energy. It is noted that the value is much larger than that expected for a simple diffusive process or viscous flow, and the large value of E_1 may be taken as an indication of the complexity of the crystallization kinetics on which such factors as diffusion, nucleation mechanisms and interface processes may exert an influence.

The activation energies for stages 2 and 3 of the crystallization process are similar in value and significantly lower than E_1. The M-phase (stage 1) appears to nucleate homogeneously whereas there is clear evidence that Ni_3Nb (stage 2) nucleates heterogeneously at the M/glass interface (Fig. 10). Heterogeneous nucleation will significantly reduce the activation energy for nucleation and is probably

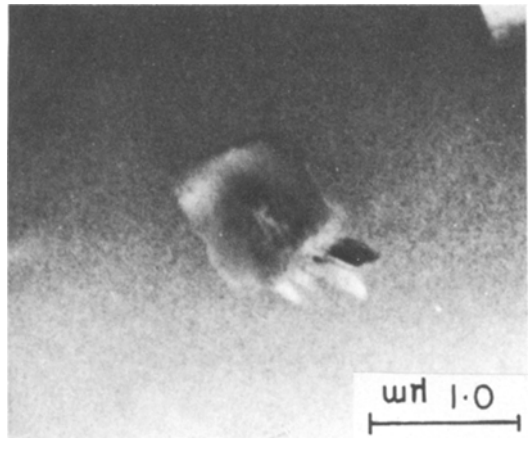

Figure 10 Bright field TEM micrograph showing nucleation of the Ni_3Nb phase at the M/glass interface, (1000 min at 845 K).

responsible for the lower value of E_2. Although the nature of the third stage of crystallization has not been experimentally determined, it seems probable that the low value of the stage 3 activation energy is also a consequence of the heterogeneous nucleation of the μ-phase.

The value of the Avrami exponent $n = 1.3$ for the crystallization of M is much smaller than the n values of 3.0 to 4.0 observed during the crystallization of many metallic glasses [22]. Values of $n = 1.3$ to 2.2 have been reported in $Fe_{80}(B, P)_{20}$ alloys [23–26], $n = 1.5$ for the crystallization of Pd–Ni–P glasses [27], and $n = 1.7$ for the initial stage of crystallization of $Fe_{32}Ni_{36}Cr_{14}P_{12}B_6$ [28]. The crystallization of $Fe_{80}(B, P)_{20}$ alloys is a complex process involving the formation of spherulites containing platelets of Fe_3B and α-Fe [29] and is not directly comparable to the results of the present study which involves the formation of a single phase. Values of $n = 1.5$ are often indicative of the diffusion-controlled growth of crystals of negligible initial dimensions [30] as is the case for the formation of fine f c c crystals in Pd–Ni–P alloys [27]. Ham [31] has shown that values of n between 1.0 and 1.5 satisfy the kinetics of a process governed by the diffusion-controlled growth of species of non-negligible initial size. Such a model does not fit the observed microstructural changes in the present study. Clearly nucleation continued throughout the time span of the observations and it was apparent that the fraction transformed during stage 1 is governed by both nucleation and growth rates.

The crystallization of the primary α-phase in $Fe_{32}Ni_{36}Cr_{14}P_{12}B_6$ most closely resembles the crystallization of M in $Ni_{60}Nb_{40}$. In that system α particles continued to nucleate at a constant rate and their growth appeared to be diffusion-controlled. In interpreting the observed value of $n = 1.7$ in that system [28, 32] attention was drawn to the calculations of Ilschner [33] whose refined model of the Avrami kinetics predicts $1 < n < 1.2$ for parabolic growth and zero nucleation rate and $n = 1.7$ for parabolic growth with a constant nucleation rate. In view of the similarity of the observed crystallization behaviour in $Fe_{32}Ni_{36}Cr_{14}P_{12}B_6$ and $Ni_{60}Nb_{40}$, and considering the calculations of Ilschner, it does not seem unreasonable to suggest that the value of $n = 1.3$ determined for the crystallization of M in $Ni_{60}Nb_{40}$ is indicative of a process involving the diffusion-controlled growth of crystals nucleating at a decreasing rate with time. Unfortunately thin foils for TEM examination could not be prepared with sufficiently uniform thickness to allow determination of the nucleation rates. However, the observation of parabolic crystal growth (Fig. 6) does support the suggestion that growth is diffusion-controlled.

4.3. The diffusion coefficient

Based on the assumption of diffusion-controlled growth, the diffusion coefficient in $Ni_{60}Nb_{40}$ was estimated to be $D = 4.2 \times 10^{-20}$ m^2 sec^{-1}. Although some error is introduced into the calculation due to uncertainty of the actual composition of the matrix phase at the interface and of the M-phase, and due to the nonspherical shape of the crystallites, the calculated value is believed to be a reasonable order of magnitude estimate.

In the only other metal–metal glass in which such a calculation has been reported, Freed and Vander Sande [34] obtained a value of $D = 5.3 \times 10^{-19}$ m^2 sec^{-1} in $Cu_{56}Zr_{44}$ glass. The equation which they used in determining D differs slightly from Equation 6 used in the present study. If an appropriate correction is made, their value $D_{CuZr} = 1.59 \times 10^{-19}$ m^2 sec^{-1} is in good agreement with the present results.

Diffusion measurements in metal–metalloid glasses appear to indicate different mechanisms for the diffusion of small metalloid atoms and the larger transition metal atoms [35]. As nickel and niobium atoms are of similar size the present results are best compared with data for the diffusion of the larger metal atoms in metal–metalloid glasses. Although all reported diffusion experiments have been performed at lower T/T_X than in the present study, it is interesting to note that extrapolation of results in other systems to $T/T_X = 0.95$ (as used in this study) suggests values of D between 10^{-19} and 10^{-20} m^2 sec^{-1}, also in good agreement with the present results.

Recent measurements [35] of the diffusion of boron in $Ni_{59.5}Nb_{40.5}$ give values of D almost three orders of magnitude larger than the values obtained here. This large difference in diffusion rates lends support to the suggestion that the smaller metalloid atoms diffuse through the structure by a different mechanism than the larger metal elements.

5. Conclusions

Crystallization of $Ni_{60}Nb_{40}$ glass appears to occur

in a 4 step process. The rapidly quenched glass partially transforms to a metastable microcrystalline phase with structure similar to that of the M-phase in the Ni–Nb–Al ternary system. During two subsequent crystallization events the remaining glass is transformed to the equilibrium Ni_3Nb- and μ-phases. The M-phase remains stable to high temperature ($\simeq 1050$ K) before transforming to the equilibrium phases. A similar crystallization sequence was observed over a wide range of temperatures and was unchanged by prior heat treatment of the glass.

Crystallization of the M phase could be described by Johnson–Mehl–Avrami kinetics with the time exponent $n = 1.3$ and activation energy $E_1 = 628$ kJ mol^{-1}. Crystal growth was apparently diffusion controlled and the diffusion coefficient was estimated to be 4.2×10^{-20} m^2 sec^{-1} at $T/T_X = 0.95$.

Activation energies for the second and third stages of crystallization were found to be $E_2 = 446$ kJ mol^{-1} and $E_3 = 430$ kJ mol^{-1}. The lower activation energies for stages 2 and 3, as compared to stage 1, may be a consequence of the heterogeneous nucleation of the Ni_3Nb- and μ-phases whereas M apparently nucleated homogeneously.

Acknowledgements

The authors wish to thank C. Ashdown for his help in the preparation of the $Ni_{60}Nb_{40}$ ribbon. The excellent facilities of the Center for Materials Science and Engineering (NSF-MRL) at MIT were extensively used for this study. This project was supported by the Army Research Office (Contract Numbers DAAG29-79-C-0077 and DAAG-29-80-K-0088).

References

1. R. C. RUHL, B. C. GIESSEN, M. COHEN and N. J. GRANT, *Acta Metall.* **15** (1967) 1693.
2. B. C. GIESSEN, M. MADHAVA, D. E. POLK and J. VANDER SANDE, *Mater. Sci. Eng.* **23** (1976) 145.
3. H. E. KISSINGER, *Anal. Chem.* **29** (1957) 1702.
4. J. A. LEAKE and A. L. GREER, *J. Non-Cryst. Solids* **38–39** (1980) 735.
5. H. J. GÜNTHERODT, M. MÜLLER, R. OBERLE, E. HAUSER, H. U. KÜNZI, M. LIARD and R. MÜLLER, "Transition Metals, 1977" edited by M. J. G. Lee, J. M. Perz and E. Fawcett, (American Institute of Physics, New York, 1978) p. 436.
6. C. B. SHOEMAKER and D. P. SHOEMAKER, *Acta Crystallogr.* **23** (1967) 231.
7. J. S. BENJAMIN, B. C. GIESSEN and N. J. GRANT, *Trans. AIME* **236** (1966) 225.
8. M. C. FLEMINGS, "Solidification Processing" (McGraw-Hill, New York, 1974) p. 74.
9. J. BURKE, "The Kinetics of Phase Transformations in Metals" (Pergamon, New York, 1965).
10. D. W. HENDERSON, *J. Non-Cryst. Solids* **30** (1979) 301.
11. H. B. AARON, D. FAINSTEIN and G. R. KOTTER, *J. Appl. Phys.* **41** (1970) 4404.
12. C. SURYANARAYANA, *Suppl. to Sci. Rep. RITU*, **A28** (1980) 143.
13. D. TURNBULL, *Solid State Phys.* **3** (1956) 225.
14. D. E. POLK, C. E. DUBE and B. C. GIESSEN, Proceedings of the 3rd International Conference on Rapidly Quenched Metals Vol. 1. Brighton, July 1978, (The Metals Society, London, 1978) p. 220.
15. L. COLLINS, PhD thesis, (MIT, Cambridge, Massachusetts, 1981) p. 99.
16. N. A. PRATTEN and M. G. SCOTT, *Scr. Metall.* **12** (1978) 137.
17. M. G. SCOTT, *J. Mater. Sci.* **13** (1978) 291.
18. H. S. CHEN, *Appl. Phys. Lett.* **29** (1976) 12.
19. C. ANTONIONE, L. BATTEZZATI, A. LUCCI, G. RIONTINO and G. VENTURELLO, *Scr. Metall.* **12** (1978) 1011.
20. J. MEGUSAR and N. J. GRANT, *Mater. Sci. Eng.* **49** (1981) 275.
21. T. HIRATA, *J. Non-Cryst. Solids* **41** (1980) 225.
22. M. SCOTT, Proceedings of the 3rd International Conference on Rapidly Quenched Metals Vol. 1, Brighton, July 1978, (The Metals Society, London, 1978) p. 198.
23. J. OREHOTSKY, *Metall. Trans. A* **11A** (1980) 1761.
24. *Idem, J. Appl. Phys.* **50** (1979) 7612.
25. A. S. SCHAAFSMA, H. SNIJDERS and F. VAN DER WOUDE, Proceedings of the 3rd International Conference on Rapidly Quenched Metals Vol. 1 Brighton, July 1978 (The Metals Society, London, 1978) p. 428.
26. Z. WRONSKI, J. SUWALSKI and H. MATYJA, Proceedings of the 3rd International Conference on Rapidly Quenched Metals Vol. 1 Brighton, July 1978 (The Metals Society, London, 1978) p. 397.
27. P. G. BOSWELL, *Scr. Metall.* **11** (1977) 701.
28. M. VON HEIMENDAHL and G. KUGLSTATTER, *J. Mater. Sci.* **16** (1981) 2405.
29. A. L. GREER and J. A. LEAKE, Proceedings of the 3rd International Conference on Rapidly Quenched Metals Vol. 1 Brighton, July 1978, (The Metals Society, London, 1978) p. 229.
30. J. W. CHRISTIAN, "Transformations in Metals and Alloys", Part 1, 2nd edn. (Pergamon, New York, 1975) p. 542.
31. F. S. HAM, *J. Phys. Chem. Solids* **6** (1958) 335.
32. S. RANGANATHAN and M. VON HEIMENDAHL, *J. Mater. Sci.* **16** (1981) 2401.
33. B. ILSCHNER, *Archiv f.d. Eisenhüttenwesen* **26** (1955) 59.
34. R. L. FREED and J. B. VANDER SANDE, *Acta Metall.* **28** (1980) 103.
35. M. KIJEK, M. AHNADZADEH, B. CANTOR and R. W. CAHN, *Scr. Metall.* **14** (1980) 1337.

Received 21 May
and accepted 28 June 1982